Post-transcriptional regulation of meiotic transcripts by the RNA binding protein CDM1 is associated with cytoplasmic condensate assemblies

Surendra Saddala[1], Neha Shukla[1], Jaroslav Fulnecek[1], Albert Cairo[1], Jakub Brolik[1], Pavlina Mikulkova[1], Jana Pecinkova[1], Ana Vargova[1], Sona Bukovcakova Valuchova[1], Claudio Capitao[2], Terezie Mandakova[1], Karel Riha[1,*]

[1]CEIITEC Masaryk University, Brno, Czech Republic

[2]Gregor Mendel Institute, Austrian Academy of Sciences, Vienna, Austria

[*]Correspondence: karel.riha@ceitec.muni.cz

Abstract

The transition from diploid to haploid life phases involves extensive changes in gene expression that drive meiotic cell division and the differentiation of haploid forms. A hallmark of meiosis is widespread post-transcriptional regulation, including delayed translation to ensure timely protein production at specific meiotic stages. Here, we describe a mechanism regulating the translation of meiotic transcripts in Arabidopsis pollen mother cells, mediated by CALLOSE DEFICIENT MICROSPORES1 (CDM1). We show that CDM1 affects several meiotic processes, including chromosome recombination, condensation, and cytokinesis. CDM1 localizes to dynamic cytoplasmic foci that closely associate with components of processing bodies and stress granules, forming three-phase condensate assemblies. Biochemical and cellular assays reveal that CDM1 is an RNA-binding protein with an intrinsic ability to drive the formation of ribonucleoprotein condensates. Furthermore, we demonstrate that CDM1 binds mRNAs present in prophase I and represses their translation until later meiotic stages, coinciding with the disassembly of CDM1 condensates. These findings identify CDM1 as a post-transcriptional regulator that fine-tunes the expression of meiotic genes to ensure proper progression of microsporogenesis.

Introduction

Meiosis is a specialized cellular process that enables the transition from diploid to haploid life forms through reductional cell division. During meiosis, a single diploid cell undergoes two consecutive rounds of chromosome segregation, producing four haploid cells. Depending on the organism's sexual life cycle, these haploid cells may differentiate into gametes or develop into diverse multicellular structures. Thus, meiosis represents an important life cycle transition, marked by extensive changes in gene expression that drive both the execution of the meiotic program and the subsequent differentiation of haploid forms.

Compared to mitosis, which typically takes only tens of minutes, meiosis is a considerably slower process, often extending over several days [1-4]. In some organisms, meiosis can pause and resume after prolonged periods, lasting months in the pollen mother cells of larch or even years in the case of human oocytes [5, 6]. Structural changes in meiotic chromosome organization during the extended prophase I partially restrict transcription [7, 8], a limitation that is compensated by post-transcriptional mechanisms, which play a key role in fine-tuning the expression of specific transcripts required for meiotic progression and post-meiotic development [9-11].

Ribosome profiling in budding yeast has revealed that translation of many transcripts produced during prophase I is delayed until later meiotic stages [12]. A prominent example is Clb3, a meiosis II-specific cyclin whose mRNA is translationally repressed during earlier stages of meiosis by the RNA-binding protein Rim4 [13]. This repression is mediated through the sequestration of transcripts into amyloid-like aggregates, preventing premature translation [14, 15]. The stabilization of meiotically produced mRNAs and their delayed translation is also hallmark of meiosis in mammals. For instance, during spermatogenesis, many genes involved in late meiotic processes are transcribed at early meiotic prophase, and mRNAs required for post-meiotic sperm differentiation are produced already during pachytene [16]. Post-transcriptional gene regulation is equally important for development of oocytes. Mammalian oocytes are transcriptionally inactive and the completion of meiosis as well as early embryonic development relies on maternally synthesized mRNAs [17]. These mRNAs are stored in mitochondria-associated ribonucleoprotein compartments formed by the RNA-binding protein ZAR1 [18].

Post-transcriptional regulation of meiotic gene expression is much less explored in plants, yet emerging evidence highlight its critical role in plant germline differentiation. In European larch, male meiosis enters a prolonged arrest during diplotene over winter, characterized by periodic chromatin relaxation accompanied by episodic transcriptional activity [5]. These transcripts are not fully spliced, but retained in nuclear Cajal bodies, preventing their premature translation until meiosis resumes [19]. This

mechanism underscores how post-transcriptional control ensures temporal precision in gene expression, aligning meiotic progression with seasonal changes. Similarly, allele-specific transcriptomics in maize revealed that transcripts generated in diploid pollen precursor cells persist in haploid microspores for up to 11 days post-meiosis [20], suggesting a strategy of mRNA storage and delayed processing that supports post-meiotic development. However, the underlying molecular mechanisms remain unknown.

Post-transcriptional regulation also governs the exit from meiosis and transition to post-meiotic development in Arabidopsis. This transition is regulated by meiotic (M) bodies, cytoplasmic condensates composed of a processing (P) body core surrounded by a stress granule-like shell [21]. At the end of meiosis, M-bodies transiently sequester translation initiation factor eIFiso4G2 via the meiosis-specific protein TDM1, thereby temporarily repressing translation to facilitate termination of the meiotic program [22]. TDM1 is recruited to M-bodies by SMG7, an evolutionary conserved nonsense-mediated RNA decay factor that acts as an adaptor protein involved in P-body remodeling and regulation of its size homeostasis [21]. The SMG7-TDM1 module is negatively regulated by meiosis I specific cyclin TAM, ensuring that meiotic exit does not occur prematurely during interkinesis [23-25].

In this study, we describe a mechanism that delays the expression of meiotically produced transcripts during *Arabidopsis* microsporogenesis, mediated by CALLOSE DEFECTIVE MICROSPORE1 (CDM1; AGI gene code At1G68200; also known under alternative name C3H15). CDM1 belongs to the family of tandem CCCH-type zinc-finger proteins [26]. Previous work has shown that CDM1 affects callose metabolism during microsporogenesis, and that its inactivation leads to abortive microspore development and male sterility [27]. Here, we show that CDM1's function extends beyond callose metabolism, influencing multiple meiotic processes including homologous recombination, chromosome condensation, and cytokinesis. CDM1 localizes to dynamic cytoplasmic speckles that are most prominent during prophase I. These speckles closely associate with M-bodies, forming three-phase condensate assemblies, suggesting a coordinated role in post-transcriptional regulation during meiosis. We further demonstrate that CDM1 binds mRNAs transcribed during prophase I and represses their translation until subsequent meiotic stages. These results indicate that CDM1 acts as a post-transcriptional regulator, fine-tuning the expression of meiotically expressed genes to ensure proper progression of microsporogenesis.

Results and Discussion

CDM1 deficiency affects multiple meiotic processes

To identify regulators of meiotic progression in Arabidopsis, we performed a suppressor genetic screen in *Arabidopsis smg7-6* mutants, which are deficient in meiotic exit and exhibit a tenfold decrease in

viable pollen along with reduced fertility [28, 29]. Screening an ethyl methanesulfonate (EMS)-mutagenized *smg7-6* population for increased seed yield revealed a line that restored the viable pollen count to wild-type levels (Fig. S1). Further genetic analyses and association mapping identified a recessive mutation in the CDM1 gene as the most likely causative variant (Fig. S1). This mutation results in a substitution of proline with serine at position 152. Plants carrying the homozygous mutant allele, designated *cdm1-2*, do not exhibit any apparent phenotype aside from rescuing meiotic progression in the *smg7-6* background (Fig. S1).

A previous study characterized a T-DNA insertion allele (*cdm1-1*) that disrupts the CDM1 gene between the C-terminal zinc-finger motifs [27]. While that study reported reduced pollen count as well as aberrant callose deposition and dissolution during the tetrad stage, meiosis was not characterized in detail. Our analysis of *cdm1-1* mutants revealed a drastic reduction in the number of viable pollen, some of which appeared larger compared to the wild type (Fig. 1a,b). The mutants were almost completely infertile, and the few viable seeds that were recovered were also substantially larger (Fig. 1c). Callose staining revealed multiple cytokinetic defects. First, we observed initiation of premature cytokinesis during meiotic interphase that was not fully completed (Fig. 1d). This was confirmed by analysis using a plasma membrane marker line (*SYP132:GFP*), which showed plasma membrane invaginations at the equatorial plate during interkinesis but no full separation of the segregated nuclei (Fig. S2). Second, the callose cell wall was thinner at the tetrad stage, confirming its aberrant deposition. Finally, we observed that some haploid nuclei at the tetrad stage were not separated by a cell wall, resulting in binuclear tetrad cells (Fig. 1d).

Cytokinesis in Arabidopsis male meiosis occurs simultaneously after completion of both nuclear divisions and is characterized by centripetal infurrowing of the primary cell wall. The position of the future cell wall is directed by microtubule structures called radial microtubule arrays (RMAs), which interconnect all haploid nuclei [30]. In some *cdm1-1* meiocytes, we observed RMAs forming between only two or three nuclei (Fig. 1e), which could explain the formation of binuclear tetrad cells (Fig. 1d).

We next performed chromosome spreads to examine whether CDM1 affects meiotic processes other than cytokinesis. This analysis revealed that chromosomes at diakinesis appeared less condensed than in the wild type and exhibited associations between heterologous bivalents (Fig. 1f). These inter-bivalent associations were also apparent when chromosomes were fully condensed at metaphase I (Fig. 1f) and may result from ectopic recombination events between heterologous chromosomes. Together, our detailed phenotypic analysis of *cdm1-1* mutants demonstrates that the function of CDM1 is not limited to callose metabolism at the end of meiosis, as previously reported [27], but influences multiple meiotic processes, including chromosome organization during prophase I.

CDM1 forms dynamic cytoplasmic speckles associated with M-bodies

To further investigate the meiotic function of CDM1, we performed expression and intracellular localization studies. We generated C-terminal fusions of the CDM1 gene, including its promoter, to GUS, GFP, and RFP reporters. All reporter constructs restored fertility in *cdm1-1* mutants, confirming their functionality (Fig. S3). The *CDM1:GUS* construct showed patchy expression in the vasculature of roots of young seedlings, as well as strong staining in anthers of floral buds at the meiotic stage (Fig. S3). The staining disappeared in older floral buds and open flowers, indicating that CDM1 expression is restricted to meiosis. This expression pattern is consistent with previous observations obtained using *pCDM1::GUS* promoter fusion constructs [31].

To examine CDM1 subcellular dynamics, we performed live imaging of pollen mother cells in CDM1-GFP plants (Video 1). The GFP signal appeared at early prophase I, forming cytoplasmic foci that were most prominent during mid-prophase I and dissolved following nuclear envelope breakdown at the onset of chromosome segregation. The signal was no longer detectable by the end of meiosis. To gain more detailed insights, we conducted confocal microscopy on fixed pollen mother cells with chromosomes counterstained with DAPI (Fig. 2a). This analysis confirmed prominent speckles during zygotene and pachytene, with both their number and size decreasing as cells progressed through metaphase I into meiosis II (Fig. 2b,c). Although some foci persisted in later stages, the CDM1 partition coefficient, which measures the signal ratio between foci and cytoplasm, declined (Fig. 2d), consistent with the partial dissolution observed in live imaging (Video 1). Notably, a portion of CDM1 appeared to relocalize to the spindle during meiosis I and II (Fig. 2a). Collectively, these data demonstrate that CDM1 exhibits a highly dynamic localization pattern, forming prominent cytoplasmic foci during prophase I and redistributing to the cytoplasm and spindle during chromosome segregation. Although *cdm1-1* mutants are female fertile [27], CDM1 is also expressed in megaspore mother cells, where it forms similar cytoplasmic foci (Fig. S4).

We next assessed whether CDM1 speckles associate with M-bodies. To this end, we performed pairwise co-localization of CDM1 with P-body markers (SMG7-TagRFP and DCP1-GFP), which label the M-body core, and with the stress granule marker TagRFP-RBP47, which localizes to the surrounding shell [21]. Confocal microscopy in pachytene meiocytes revealed extensive co-localization of CDM1 foci with all three markers, indicating a close association with M-bodies (Fig. 3a–i). However, closer inspection suggested that CDM1 signals were juxtaposed rather than fully overlapping with the P-body markers (Fig. 3b,d). In contrast, overlap with TagRFP-RBP47 was more pronounced (Fig. 3f), consistent with CDM1 localization to the M-body shell.

To refine these observations, we used structured illumination microscopy. This analysis confirmed that CDM1 and SMG7 occupy adjacent, non-overlapping domains, with CDM1 foci encircling the SMG7-labeled core (Fig. 3j). Surprisingly, CDM1 did not fully co-localize with RBP47 either (Fig. 3k). Three-dimensional rendering revealed that CDM1 and RBP47 form distinct but intermingled patches surrounding the presumed M-body core (Fig. 3k). Together, these results suggest that pachytene M-bodies are three-phase condensates, composed of a P-body core surrounded by discrete, interspersed stress granule-like and CDM1 condensates.

CDM1 represses translation of late meiotic proteins during prophase I

The pleiotropic effects of CDM1 on meiosis, its localization to cytoplasmic speckles, and the previously reported RNA-binding capacity of the closely related Arabidopsis protein C3H14 [32] suggested that CDM1 may bind RNA and regulate meiotically expressed transcripts. To identify potential targets of CDM1 regulation, we performed CDM1:GFP immunoprecipitation from meiotic floral buds using anti-GFP nanobeads, followed by sequencing of the co-purified RNA. Genes enriched in the CDM1:GFP RIP-seq compared with the wild-type RIP-seq control (Table S1) were further filtered based on altered expression in *cdm1-1* mutants in microarray data [27] and specific expression in floral buds, according to the Arabidopsis transcriptome database (https://travadb.org/) [33]. Two preselected candidates, G3BP5 (At3g07250) and BT3 (At1g05690), were validated by RIP-qPCR for association with CDM1:GFP (Fig. 4a) and by qRT-PCR as being downregulated in *cdm1-1* mutants (Fig. 4b) and were analyzed further.

To monitor G3BP5 and BT3 protein expression during meiosis, we generated genic constructs containing their promoter regions fused to eYFP at the C-terminus. In wild type, G3BP5:eYFP showed little to no signal during meiosis I, with expression rising in tetrads and peaking in microspores (Fig. 4c). BT3:eYFP displayed a similar pattern, remaining low through meiosis I and increasing in tetrads and microspores (Fig. 4d). In *cdm1-1*, however, both proteins accumulated earlier and at higher levels. G3BP5:eYFP was already prominent at pachytene, reached a maximum at metaphase I, and declined by the microspore stage (Fig. 4c,e). BT3:eYFP in *cdm1-1* formed distinct cytoplasmic foci, first visible at pachytene, with peak intensity at telophase II and the tetrad stage, followed by a decrease in microspores (Fig. 4d,f). These foci, absent in wild-type meiocytes, may represent aggregates of overproduced protein.

To determine whether CDM1 regulates *G3BP5* and *BT3* expression at the transcriptional or post-transcriptional level, we performed single-molecule RNA FISH in pachytene meiocytes. For *G3BP5*, we detected an average of ~400 foci per cell, with ~300 in the cytoplasm and ~100 in the nucleus (Fig. 5a,b). In *cdm1-1* mutants, cytoplasmic foci were significantly reduced, whereas nuclear foci remained unchanged. A similar pattern was observed for BT3 transcripts, which were less abundant than G3BP5

mRNAs but likewise showed a marked reduction in the absence of CDM1 (Fig. 5c,d). These findings indicate that *G3BP5* and *BT3* mRNAs are already present during pachytene, where they are translationally repressed and likely stabilized by CDM1. Loss of CDM1 appears to relieve this repression, resulting in strong protein accumulation (Fig. 4c–f). This premature translation may deplete the mRNA pool during prophase I, consistent with the reduced transcript numbers (Fig. 5) and lower protein levels at the end of meiosis (Fig. 4c–f). Thus, CDM1 functions as a translational repressor, delaying expression of late meiotic and post-meiotic proteins from mRNAs synthesized during early meiotic stages.

CDM1 is an RNA binding protein with propensity to form molecular biocondensates

The role of CDM1 in translational repression suggests that it may directly bind to its target mRNAs. To test this, we performed RNA electrophoretic mobility shift assays (REMSA) using *E. coli* - expressed CDM1 and the *in vitro* transcribed 5'UTR of G3BP5 mRNA, as UTRs are known as interaction hubs for translational regulators [34]. Because heterologously expressed CDM1 tends to aggregate, it was fused to maltose-binding protein (MBP) to improve *in vitro* solubility. REMSA with three oligoribonucleotides spanning different regions of the 5'UTR revealed a CDM1-dependent mobility shift with probe 5'-1, corresponding to the 77 nt at the 5' terminus (Fig. S5 and Fig. 6a). Competition assays with excess unlabeled RNAs confirmed the high specificity of this interaction (Fig. 6a), demonstrating that CDM1 can specifically bind the 5'UTR of its target RNA.

The localization of CDM1 to cytoplasmic speckles and its tendency to aggregate prompted us to test whether it can homomultimerize. *In vitro* immunoprecipitation using soluble MBP-CDM1 fusion proteins revealed that CDM1 forms dimers or higher-order multimers (Fig. 6b), and a specific self-interaction was also confirmed by yeast two-hybrid assay (Fig. S6). To assess interactions in plant cells, we performed bimolecular fluorescence complementation (BiFC) in mesophyll protoplasts. Heterologously expressed CDM1-GFP formed prominent cytoplasmic speckles resembling those in pollen mother cells (Fig. 6c). Co-transfection with bimolecular complementation constructs produced similar foci, indicating direct interaction or close spatial association of CDM1 molecules within these structures.

Close association of CDM1 speckles with P-bodies and stress granules in the form of multiphasic M-bodies, suggests that CDM1 can assemble into biocondensates with properties of liquid-liquid phase-separated droplets. One hallmark of such droplets is their ability to fuse, a property observed for CDM1 speckles both in meiocytes and in heterologously expressed CDM1 speckles in mesophyll protoplasts (Fig. 7a). Another defining feature is the high mobility of their constituents. Fluorescence recovery

after photobleaching (FRAP) experiments showed partial restoration of the CDM1-GFP signal, indicating exchange of CDM1 molecules with the surrounding cytoplasm (Fig. 7b,c).

To determine whether CDM1 possesses intrinsic phase-separation capabilities, we performed *in vitro* droplet formation assays using MBP-CDM1-GFP fusion protein. Cleavage of the MBP solubility tag induced the formation of liquid droplets, whose size increased with protein concentration (Fig. 7d). To test the influence of RNA, we repeated the assay in the presence of G3BP5 RNA. RNA facilitated CDM1 phase separation, producing larger droplets at 1 µM and 2.5 µM concentrations compared with corresponding controls lacking RNA (Fig. 7d,e). Notably, CDM1 formed biphasic condensates in the presence of RNA (Fig. 7e), suggesting the existence of two demixed populations, potentially representing RNA-bound and RNA-free configurations.

Together, these results demonstrate that CDM1 speckles in plant cells exhibit characteristics of liquid-liquid phase-separated droplets, driven by an intrinsic ability of CDM1 to nucleate such structures, particularly in the presence of RNA.

Materials and Methods

Plant material and growth conditions

Arabidopsis thaliana ecotype Col-0, mutant lines, and transgenic lines were grown on soil in controlled growth chambers under long-day conditions (16 h light/ 8 h dark) at 21 °C and 50-60% relative humidity. For heat shock treatments, whole inflorescences were immersed in liquid ½ Murashige and Skoog (MS) medium supplemented with 5% sucrose in 1.5 mL tubes and incubated at 39 °C for 20 minutes using a heat block.

Suppressor screen

The suppressor screen for identifying mutations that restore fertility in *smg7-6* mutant plants was performed as previously described[28]. Causal *de novo* mutations associated with the suppressor phenotype were identified by whole-genome sequencing and mapped using the ArtMAP pipeline [35].

To genotype the *smg7-6* background in the EMS105 (*cdm1-2*) suppressor line, two primer pairs were used: SMG7-6_F and SMG7-6_R to detect the wild-type allele, and SMG7-6_R with LBa1 to confirm the T-DNA insertion (Table S2). The EMS105 point mutation was genotyped using the High-Resolution Melting (HRM) analysis method with primers HRM_EMSCDM1105_F and HRM_EMSCDM1105_R (Table S2).

Reporter lines used in this study

The following *Arabidopsis* mutant lines were used in this study: *smg7-6* [36] and *cdm1-1* (SALK_065040)[27]. The *cdm1-1* T-DNA insertion line was obtained from the NASC seed stock center. Genotyping was

performed using primers CDM1.1 LP+RP and CDM1.1 LP+LBb1.3 (Table S2). Note: SALK_065040 contains an inverted tandem insertion of the LBb1.3 T-DNA border, which may produce PCR products with both gene-specific primer; optimal primer combinations were selected based on empirical PCR conditions.

The following *Arabidopsis* reporter lines were used in this study: SMG7-TagRFP[22], DCP1-G3GFP, and TagRFP-RBP47b [21]. The following reporter lines were generated by this study: *CDM1p::CDM1:GUS (cdm1-1)*, *CDM1p::CDM1:G3GFP (cdm1-1)*, and *CDM1p::CDM1:TagRFP (cdm1-1), G3BP5p:: G3BP5:eYFP (cdm1-1), BT3p:: BT3:eYFP (cdm1-1)*. Constructs used in protoplast assays included *35Sp::CDM1:G3GFP* and *35Sp::CDM1:nYFP*, *35Sp::CDM1:cYFP,* while *His$_6$-MBP-CDM1* and *His$_6$-MBP-CDM1-G3GFP* were used for biochemical analyses. Notably, N-terminal fusions of CDM1 to fluorescent proteins were non-functional (data not shown); therefore, all localization and condensate assays were performed using C-terminally tagged CDM1 constructs.

By crossing *cdm1-1* with the *HTA10:RFP* and *SYP132-GFP* marker lines, the following genotypes were generated: *WT (HTA10:RFP)*, *cdm1-1 (HTA10:RFP)*, *WT (HTA10:RFP;SYP132-GFP)*, and *cdm1-1 (HTA10:RFP;SYP132-GFP)*.

Plasmid construction and generation of transgenic Arabidopsis lines

Primer sequences used for plasmid construction are listed in Table S2. All constructs were generated using Gateway® cloning technology (Invitrogen) and destination vectors from the pGWB series[37]. The genomic sequence of *CDM1*, including 1500 bp upstream of the start codon (native promoter) but excluding the stop codon, was amplified using primers pCDM1-F and CDM1-RSTOP-. The PCR product was cloned into the pENTR™/D-TOPO™ vector (Invitrogen, cat. no. 45-0218) to generate an entry clone, which was subsequently recombined into pGWB633, pGWB650, and pGWB659 by LR reactions (Invitrogen, cat. no. 11791-020), resulting in the native promoter-driven constructs *CDMp::CDM1-GUS*, *CDMp::CDM1-G3GFP*, and *CDMp::CDM1-TagRFP*, respectively. Genotyping primers for these transgenes are provided in Table S2.

To obtain a coding-sequence-only version of *CDM1* (without introns and stop codon), primers CDM1-F and CDM1-RSTOP− were used to amplify the cDNA from floral tissue. The product was cloned into pENTR™/D-TOPO™, and the resulting entry clone was used in LR reactions with BiFC-compatible destination vectors pGWnY and pGWcY, generating the constructs *35Sp::CDM1CDS:nYFP* and *35Sp::CDM1CDS:cYFP*, respectively. The same CDM1 entry clone was used in an LR reaction with the destination vector pGWB651 to generate the *35Sp::CDM1:G3GFP* construct for expression in protoplasts.

For bacterial expression, DNA fragments were amplified from the *35Sp::CDM1:G3GFP* plasmid using two different primer sets. The first set, CDM1-F and G3GFP-R, was used to generate the *CDM1-G3GFP* fragment, while the second set, CDM1-F and CDM1-RSTOP-, was used to amplify the *CDM1* coding region without the stop codon. PCR products were cloned into the SspI-linearized pET His_6-MBP-TEV LIC vector (1M). The resulting constructs, *His_6-MBP-CDM1-G3GFP* and *His_6-MBP-CDM1*, were digested with DpnI and transformed into *E. coli* BL21-Rosetta cells for protein expression in LB medium containing kanamycin.

Additionally, the genomic sequence of *G3BP5*, including 1500 bp upstream of the start codon and lacking the stop codon, was amplified with primers pG3BP5-F and G3BP5-RSTOP−. The entry clone was recombined into pGWB640 to produce the *G3BP5p::G3BP5-eYFP* construct. Similarly, *BT3* was amplified using pBT3-F and BT3-RSTOP−, and the resulting entry clone was used to generate *BT3p::BT3-eYFP* via recombination into pGWB640.

DAPI and callose staining

To assess meiotic and cytokinetic defects, 0.3–0.6 mm floral buds were fixed in 4% formaldehyde in MTSB (50 mM PIPES, 5 mM EGTA, 5 mM $MgSO_4$, pH 6.9, 0.1% Triton X-100) under vacuum for 15 minutes on and 45 minutes off. Samples were washed three times with MTSB (5 min each), and anthers were dissected and transferred into fresh tubes using cut 200 µL pipette tips.

Staining was performed with 2 mg/mL DAPI or Renaissance in MTSB for 1 hour at room temperature in the dark. Samples were centrifuged (400g, 30 sec), washed twice with MTSB, and incubated in 100 µL fresh MTSB at 60 °C for 10 minutes, followed by 10 minutes on ice and a final MTSB wash. One last wash is given with 1ml of MTSB. Samples were centrifuged (400g, 30 sec). Anthers were mounted in Vectashield (without DAPI) on glass slides, and excess medium was removed using filter paper. Coverslips were sealed with nail polish prior to imaging.

Tubulin Immunostaining

Anthers were dissected in MTSB and placed on a coverslip, then gently squashed onto a glass slide using a pencil tip. Slides were snap-frozen in liquid nitrogen, and coverslips were removed with a razor blade. After air-drying at room temperature for 1 hour, slides were rehydrated with a drop of MTSB for 5 minutes. Approximately 50 µL of 2% Driselase (Sigma-Aldrich, cat. no. D9515) in 7% (w/v) sucrose prepared in MTSB was applied to each slide, covered with parafilm, and incubated in a humid chamber at room temperature for 30 minutes.

Following enzymatic digestion, slides were washed twice with MTSB (5 minutes each) and incubated overnight at 4 °C with 150 µL of rat monoclonal anti-α-tubulin antibody (Serotec, cat. no. MCA78G)

diluted 1:1000 in MTSB. The next day, slides were incubated for 1 hour at room temperature with Cy3-conjugated goat anti-rat IgG secondary antibody (Chemicon, cat. no. AP183C) diluted 1:1000 in MTSB. Slides were washed three times with 200 µL of MTSB, mounted in Vectashield containing DAPI, and sealed with clear nail polish after removing excess mounting medium with Whatman filter paper.

GUS staining

Tissues (one-week old seedlings and inflorescences from wild-type and *CDM1p::CDM1:GUS* transgenic plants) were fixed in 4% formaldehyde in 1X PBS, washed in 0.1 M sodium phosphate buffer (pH 7.0). Tissues were incubated in GUS staining buffer (100 mM sodium phosphate buffer; pH-7.0, 10 mM EDTA; pH-8.0, 0.1% Triton X-100, 1 mM X-Gluc in DMF; 0.5 mM $K_3Fe(CN)_6$; 0.5 mM $K_4Fe(CN)_6$), and applied vacuum 15 minutes. Then, the tissues were incubated in GUS staining buffer in dark at 37 °C for 48 hours. Stained tissues were then imaged using a Zeiss Stereo Discovery.V8 microscope and images were treated in Fiji.

Cytology

Pollen count and viability were assessed using Alexander staining, described previously [38]. Samples were imaged with a Zeiss Axioscope.A1 transmitted light microscope (20×/0.5 objective), equipped with an Axiocam 105 camera and Visiview software (Visitron Systems). Meiotic progression was analyzed by DAPI staining of pollen mother cells (PMCs) in whole anthers as described by Capitao et al. [28], and imaged using a Zeiss LSM780 confocal microscope.

Anther sample preparation for protein localization

Protein localization in Arabidopsis anthers was performed as described previously [28]. 3-5 inflorescences were fixed by vacuum incubation with 4% formaldehyde in 1X PBS (Fixation Buffer -FB) for 15 min, followed by 45 min of incubation without vacuum. The sample were washed 3X5min with 1X PBS before dissecting the meiotic floral buds to isolate meiotic anthers, and then they were incubated 1 hour with 5 µg/ml DAPI in 1X PBS. Next, the anthers were washed 3 times with 1X PBS, 1 time with 1X PBS on ice, and 1 time with 1X PBS at room temperature. Finally, the anthers were placed in a microscope slide with VECTASHIELD® Antifade Mounting Media to be subsequently imaged.

Laser scanning confocal imaging

Laser scanning confocal imaging was performed in two systems. The Inverted microscope Zeiss Axio Observer.Z1 with confocal unit LSM 780 was used to image protoplasts, and anthers. For the protoplasts we used the objective LCI Plan-Neofluar 63x/1.3 1mm Korr DIC M27. For the anthers and invitro condensates, we used the objective C-Apochromat 63x/1.2 W Korr UV-VIR-IR M27.

Super-resolution imaging

Super-resolution images acquired with the ZEISS Elyra 7 system were also processed using Fiji. To obtain a resolution beyond the Abbe diffraction limit of the conventional light microscope we used the motorized inverted microscope ZEISS Elyra 7 with widefield option to acquire images of smFISH for meiocytes. We used the objective alpha Plan-Apochromat 100x/1.46 Oil DIC M27, 1.6 Lense, and the 2 x PCO edge sCMOS camera, 1280 x 1280, pixel size 6.5 µm × 6.5 µm. The raw images were acquired using a dimension of 512 x 512 pixels and 9 phases.

Live cell imaging

Live cell imaging of Arabidopsis pollen mother cells was performed using Light sheet microscopy as previously described [4]. Anthers were imaged in Light sheet Z.1 microscope (Zeiss) (Objective W Plant-Apochromat 20x/1.0 DIC) in 5 min time increments.

Image processing

All 2D image analyses were performed using Fiji. Depending on the experiment, either single optical slices or maximum intensity projections (MIPs) of five central slices were used for representative images and quantification, as detailed in the figure legends. 3D rendering of RNP granules from meiocytes was conducted in Imaris v10.2.0 using volume rendering.

Protein localization and BiFC assay in protoplasts

Arabidopsis mesophyll protoplasts were isolated and transfected as described previously with minor modifications [22, 39]. Briefly, protoplasts were prepared from leaves of 4-week-old soil-grown *Arabidopsis thaliana* cultivated under 12 h light/12 h dark cycles at 22 °C. Approximately 20-30 leaves were finely cut with a clean razor blade and digested in 15 mL of enzyme solution (which is heated at 55^0C for 10min in a water bath and cooled to room temperature for 50 min) containing 1% cellulase Onozuka R10 (Duchefa, cat. no. C8001), 0.25% macerozyme R10 (Duchefa, cat. no. M8002), 0.4 M mannitol, 20 mM KCl, and 20 mM MES (pH 5.7). The digestion was performed under vacuum for 15 minutes, followed by incubation for 3 hours in the dark at room temperature. The released protoplasts were filtered through a 70 µm mesh (Corning, cat. no. 431751), washed twice with W5 solution (154 mM NaCl, 125 mM $CaCl_2$, 5 mM KCl, 2 mM MES, pH 5.7), and kept on ice.

For transfection, protoplasts were resuspended in MMg solution (0.4 M mannitol, 15 mM $MgCl_2$, 4 mM MES, pH 5.7) at a concentration of 3 X 10^5 cells/mL. A total of 100 µL of protoplast suspension was mixed with 15 µg of plasmid DNA and 110 µL of freshly prepared PEG solution (4 g PEG 4000 [Sigma-Aldrich, cat. no. 81240], 2.5 mL of 0.8 M mannitol, 1 mL of 1 M $CaCl_2$, and 3 mL nuclease-free water). After 10 minutes of incubation in the dark at room temperature, 440 µL of W5 medium was added. The protoplasts were gently centrifuged, resuspended in fresh W5 medium, and incubated for 16 hours

in petri dish coated with Fetal Bovine Serum the dark at room temperature. Fluorescence imaging of transfected protoplasts was performed using a Zeiss LSM780 confocal microscope.

RNA immuno-Precipitation (RIP)

Approximately 50-100 mg of meiotic inflorescences were collected in a watch glass on ice from *Arabidopsis* wild-type and *CDM1p::CDM1:G3GFP* plants. After removing surface moisture with a tissue towel, buds were snap-frozen in liquid nitrogen and ground into a fine powder using a pre-chilled ceramic mortar and pestle. Lysis was initiated by adding 1 mL of ice-cold lysis buffer (50 mM Tris-HCl pH 7.5, 150 mM NaCl, 5 mM $MgCl_2$, 0.5 mM DTT, 10% glycerol, 0.05% Nonidet P-40, 1 mM PMSF, 1X protease inhibitor cocktail [cOmplete ULTRA Tablets, EDTA-free; Roche, cat. no. 05892953001], 20 U/mL RNaseOUT [Invitrogen, cat. no. 10777019]) prepared in DEPC treated, sterile MilliQ water, directly into the mortar. The mixture was thawed to 4 °C and transferred to RNase-free Protein LoBind microcentrifuge tubes. Lysates were incubated on ice for 30 minutes with occasional mixing. Samples were centrifuged at 10,000 rpm for 10 minutes at 4 °C. Protein concentration was estimated using the Bradford assay, and 1mg of totals protein extract is used for further immunoprecipitation by using ChromoTek GFP-Trap® magnetic beads.

Samples were pre-cleared before pull-down with 30ul of ChromoTek binding control beads (lacking antibody), which were equilibrated in lysis buffer and incubated with lysates on a rotating wheel at 4 °C for 45 minutes. 5% inputs of the pre-cleared lysates were stored at -20 °C. In parallel, GFP-Trap beads were equilibrated in lysis buffer. The pre-cleared lysates were incubated with calibrated 30ul of GFP-Trap beads for 90 minutes at 4 °C with rotation at 16rpm. By using a magnetic rack, the bound beads were then washed three times (5 minutes each at 4 °C) with wash buffer (50 mM Tris-HCl pH 7.5, 150 mM NaCl, 5 mM $MgCl_2$, 0.5 mM DTT, 20 U/mL RNaseOUT). The final wash was transferred into new DNA LoBind tubes to reduce carryover.

RNA Preparation and NGS Library Preparation

RNA was extracted from both input and immunoprecipitated (IP) samples by adding 1 mL of RNA Blue reagent (Top-Bio, cat. no. R013) and processing according to the manufacturer's instructions. RNA concentrations were measured using the Qubit RNA Assay Kit (Invitrogen, cat. no. Q10210), and residual DNA was removed with TURBO DNase (Invitrogen, cat. no. AM1907).

For NGS library preparation, 1–5 ng of DNA-free RNA was used. Libraries were prepared using the TruSeq Stranded Total RNA Library Prep Kit (Illumina) and indexed with IDT for Illumina TruSeq DNA and RNA UD Indexes, following the manufacturer's protocol. Sequencing was

performed on an Illumina NextSeq 500 platform using the NextSeq 500/550 High Output Kit v2.5 (75 cycles).

cDNA Preparation and qPCR Analysis

cDNA was synthesized from 500 ng of DNA-free RNA from floral buds or RNA prepared after RIP, using the SuperScript™ IV (Invitrogen, cat. no. 18090050), following the manufacturer's protocol. A mix of random hexamer primers (Thermo Scientific, cat. no. SO142) and oligo(dT) primers (Thermo Scientific, cat. no. SO132) were used for reverse transcription. Quantitative PCR (qPCR) was performed using the KAPA SYBR® FAST qPCR Kit (KAPA Biosystems, cat. no. KR0389). Primer sequences used for qPCR are listed in Table S2.

Single-molecule RNA Fluorescence In Situ Hybridization (smFISH)

smFISH was performed as previously described with few modifications [40, 41]. Briefly, inflorescences were fixed in 4% methanol-free formaldehyde (Thermo Scientific, cat. no. 28908) prepared in 1X PBST (10X PBS, Invitrogen, cat. no. AM9624, diluted in nuclease-free water [BioConcept, cat. no. 3-07F04-I] with 0.1% Triton X-100). Samples were vacuum-infiltrated (15 minutes on, 45 minutes off), and meiotic anthers were dissected under a stereo microscope.

Dissected anthers were transferred onto a clean glass slide and covered with a coverslip. Excess buffer was removed by inverting the slide onto tissue paper. Anthers were gently squashed using a pencil tip to release individual meiocytes. Slides were immediately snap-frozen in liquid nitrogen, the coverslip removed with a razor blade, and slides were air-dried at room temperature for 1 hour.

Slides were pre-hybridized (hydrated) with 150 µL of pre-hybridization buffer (Stellaris Buffer A 1X [Biosearch Technologies, cat. no. SMF-WA1-60] containing 20% [v/v] formamide (AppliChem, cat. no. A2156) in nuclease-free water) for 5 minutes in a fume hood. Hybridization was carried out overnight at 37 °C in a dark, humid chamber using 150 µL of hybridization buffer (Stellaris Hybridization Buffer [Biosearch Technologies, cat. no. SMF-HB1-10] with 10% [v/v] formamide) containing 1:100 dilution of the smFISH probe. The samples were covered with piece of inner side of a fresh autoclave bag and incubated in a dark humid chamber at 37^0C for overnight.

The next day, remove the piece of plastic, unbound probes were removed by two washes with pre-hybridization buffer at 37 °C in a dark humid chamber: the first wash for 5 minutes and the second for 25 minutes. DAPI (2 mg/mL) was diluted in pre-hybridization buffer and applied to slides (150 µL) for 30 minutes at 37 °C. Slides were then washed with 200 µL of Stellaris Wash Buffer B (Biosearch Technologies, cat. no. SMF-WB1-20) without formamide for 5 minutes and mounted in Vectashield. Coverslips were sealed with nail polish.

Image Acquisition

Images were acquired using a ZEISS Elyra 7 super-resolution microscope in widefield mode. Z-stacks were captured with a step size of 0.2 µm. For smFISH detection, the following probe and imaging settings were used: *G3BP5* or *BT3* labeled with Quasar 570 (excitation 561 nm, 10% laser power, 500 ms exposure, emission 590 nm), GAPDH labeled with Quasar 670 (excitation 642 nm, 30% laser power, 500 ms exposure, emission 655 nm), and DAPI (excitation 405 nm, 3% laser power, 100 ms exposure, emission 440 nm). Probe sequences and catalog numbers are provided in **Error! Reference source not found.**.

Quantification and statistical analysis

Quantification analysis of condensates was performed using Fiji image analysis software. Counting of viable pollen grains was performed using the Count tool in Fiji image analysis software. Data analysis and graph constructions were performed using GraphPad Prism 7 software. Significance testing was conducted with Mann-Whitney test with a significance threshold of $p < 0.05$. Further details can be found in the figure legends.

Protein expression and purification

The *His_6-MBP-CDM1-GFP* or *His_6-MBP-CDM1* construct was transformed into *E. coli* Rosetta (DE3) cells (Novagen). Protein expression was induced with 0.5 mM IPTG for 4 hours at 30 °C when the culture reached an OD_{600} of 0.4. Cells were harvested by centrifugation, and the pellet was resuspended in lysis buffer containing 0.1 M Tris-HCl (pH 7.5), 0.5 M NaCl, 0.05% Tween 20, 1% Triton X-100, 1 mg/mL lysozyme (Sigma-Aldrich, cat. no. L6876), 1 mM DTT, and 1X protease inhibitor cocktail. The suspension was sonicated and centrifuged to obtain the soluble protein extract.

The supernatant was filtered through a 0.2 µm filter (Sartorius, cat. no. 17764) and supplemented with 50 mM imidazole (Sigma-Aldrich, cat. no. I5513). His-tagged proteins were purified using His Mag Sepharose™ Ni magnetic beads (Cytiva, cat. no. 28967390) following the manufacturer's protocol. Eluted His_6-MBP-CDM1-GFP was dialyzed into storage buffer (20 mM HEPES, pH 7.4, 150 mM KCl, 1 mM DTT), however His_6-MBP-CDM1 was dialyzed in RNase free 1X PBS, concentrated using Amicon® Ultra-0.5 centrifugal filters (Merck Millipore, cat. no. UFC503024). Purified proteins were stored at −80 °C.

In vitro dimerization assay and Western blot

To assess CDM1 dimerization, 20 µg of purified His_6-MBP-CDM1-GFP protein was incubated with His_6-tagged TEV protease (Promega, cat. no. V610A) in 100 µL total volume (1X TEV buffer, 1 mM DTT, 2 µL TEV) at room temperature for 1 hour. To remove the cleaved MBP tag and TEV protease, the reaction was incubated with 10 µL His Mag Sepharose™ Ni beads for 30 minutes at room temperature, followed

by a second round of purification with fresh beads. The unbound cleaved CDM1-GFP was collected for further analysis.

For the dimerization assay, equal molar amounts of long His_6-MBP-CDM1-GFP and short CDM1-GFP were mixed in storage buffer (20 mM HEPES, pH 7.4, 150 mM KCl, 1 mM DTT) in a 50 µL reaction and incubated at room temperature for 2 hours on a rotating wheel (16 rpm). Complexes were immunoprecipitated by incubating with 1 µL anti-His antibody (Abcam, cat. no. ab18184) for 30min and Protein G-conjugated Sepharose beads (Invitrogen, cat. no. 10003D) blocked with 2% BSA for 30 min at room temperature. Beads were washed with storage buffer, resuspended in 20 µL, and stored at -20 °C along with input and unbound fractions.

Proteins were eluted with 1X Laemmli buffer and boiled prior to SDS-PAGE. Western blots were probed using rat anti-GFP antibody (Chromotek, cat. no. 3H9) and HRP-conjugated secondary antibody. Detection was performed using a luminol-based chemiluminescent substrate (Thermo Scientific, cat. no. 34095). Imaging was performed using Chemidoc system.

In vitro phase separation assay

Phase separation assays were performed in storage buffer (20 mM HEPES, pH 7.4, 150 mM KCl, 1 mM DTT) containing increasing concentrations of purified His_6-MBP-CDM1-GFP. To remove the N-terminal solubilizing His-MBP tag, proteins were treated with 0.5 U/µL TEV protease. Phase separation was induced by adding 10% (w/v) PEG8000 (Carl Roth, cat. no. 0263.2) as a crowding agent. Reactions were assembled by placing 5 µL droplets into custom-made imaging chambers constructed using double-sided tape on standard microscopy slides. To test RNA-induced phase separation, 100 ng/µL of in vitro transcribed 5' UTR RNA of *G3BP5* was added to parallel reactions. Chambers were sealed with a coverslip, inverted, and incubated in a humidified chamber at 25 °C for 10 minutes. Droplet formation was visualized using a ZEISS LSM780 confocal microscope with a C-Apochromat 63×/1.2 W Korr UV-VIS-IR M27 objective.

FRAP analysis

Fluorescence recovery after photobleaching (FRAP) was performed using a ZEISS LSM780 confocal microscope. Regions of interest (ROIs) in protoplasts and meiocytes were bleached using a 514 nm laser at 100% intensity to deplete the GFP signal. Recovery of fluorescence was monitored by time-lapse imaging over 180 seconds. Image processing and quantification were conducted on maximum intensity projections (MIPs) of Z-stacks using Fiji.

RNA Electrophoretic Mobility Shift Assay (RNA-EMSA)

Two RNA oligonucleotides representing the 5′ region of the *G3BP5* transcript were used: 5-1-1 RNA (77 nt, 23.04 kDa; nucleotides 1–75) (5′-GGUCGUCAUUUCUUAACAAAUAAGUCAUUUCUUUUGUGUUAGCCGCUGCUUCUCACCAUUUCUUUUAUGAUUAUGUU-3′) and 5-1-2 RNA (90 nt, 27.36 kDa; nucleotides 75–162) (5′-GGUCGCAAGAUCUAACGAUUUUGCGUUUGGAACUUGAUUUGAGAUACAGGGCAUUGCAUAUUCUCUGUAUCGAUGGAUCCUCGUCCAAAU-3′). DNA templates for in vitro transcription were amplified from 10 ng of plasmid DNA containing the corresponding *G3BP5* fragment using Phusion™ Hot Start II DNA Polymerase (Thermo Fisher). Primers used were: For 5-1-1 RNA: T7-1F (5′-TAATACGACTCACTATAGGTCGTCATTTCTTAACAAATAAGTCAT-3′) and 75R (5′-AACATAATCATAAAAGAAATGGTGAGA-3′), for 5-1-2 RNA: T7-75F (5′-TAATACGACTCACTATAGGTCGCAAGATCTAACGATTTTGCGTTTGG-3′) and 162R (5′-ATTTGGACGAGGATCCATCGATACAGAGAA-3′)

The PCR conditions consisted of 35 cycles at 98 °C for 10 s, at 60 °C for 10 s, and at 72 °C for 10 s. The PCR products were then purified from the agarose gels using the NucleoSpin® Gel and PCR Clean-Up Kit (Macherey-Nagel), extracted one time with phenol:chloroform:IAA (25:24:1), twice with chloroform:IAA (24:1), ethanol-precipitated, washed with 75% RNase-free ethanol, and re-suspended in 10 µL of DEPC-treated water. RNA concentrations were quantified using a NanoDrop spectrophotometer.

In vitro transcription was performed using the HiScribe T7 High Yield RNA Synthesis Kit (New England Biolabs) to generate cold competitor RNAs and radiolabeled ("hot") 5-1-1 RNA. For the radiolabeled transcript, the transcription reaction involved 1 µg of the DNA template, with α-^{32}P-UTP (3 µL, 10 mCi/mL, >6000 Ci/mmol) and subsequently removing the DNA template using the TURBO DNA-free kit (Thermo Scientific) and then purifying the RNA via RNA-blue reagent extraction (Top-Bio) followed by two chloroform:IAA extractions, ethanol precipitation, and resuspending in RNase-free PBS buffer that matched the dialysis buffer of the 6×His-MBP-CDM1 protein. RNA concentrations were quantified using Qubit 3.0 Fluorometer (Thermo Fisher).

Binding reactions (final volume of 20 µL) contained 20 nM of radiolabeled 5-1-1 RNA, increasing amounts of 6×His-MBP-CDM1 protein, 10 mM HEPES, pH 7.3, 20 mM KCl, 1 mM $MgCl_2$, 10 µM $ZnSO_4$, 1 mM DTT, 5% glycerol, 0.1 mg/mL heparin, and 0.5 U of ProTEV Plus protease (Promega). The reactions were incubated at 37 °C for 15 minutes prior to running the samples on a native 5% polyacrylamide gel (acrylamide:bis-acrylimide 29:1, Sigma) in 0.5× TBE. Gels were pre-electrophoresed in 0.5× TBE at 100 V for 1 hour at 4 °C, run with the samples at 160 V for 5 hours at 4 °C, and then dried,

exposed to phosphor screens (GE Healthcare), and scanned on a Typhoon™ FLA 7000 imaging system (GE Healthcare).

Yeast Two-Hybrid Assay

Yeast two-hybrid experiments were conducted using the Matchmaker™ GAL4-based system (Clontech). Bait and prey constructs were transformed into *Saccharomyces cerevisiae* strains Y187 and AH109, respectively. Protein-protein interactions were assayed by the mating method. Diploid yeast cells carrying both plasmids were selected on SD/-Leu/-Trp medium and screened for interactions on SD/-Leu/-Trp/-His supplemented with 2.5 mM 3-amino-1,2,4-triazole (3-AT) at 30 °C. Empty vector combinations served as negative controls to test for auto-activation. Each assay was performed in triplicate, with two technical replicates per experiment.

Acknowledgements

This work was supported by the Czech Science Foundation (EXPRO grant 23-07969X). We further acknowledge the core facilities of CEITEC Masaryk University for support in obtaining and analysing scientific data: CELLIM funded by MEYS CR (LM2023050 Czech-BioImaging), and Plant Science Core Facility.

References

1. Bennett, M.D. The time and duration of meiosis. *Philos Trans R Soc Lond B Biol Sci* **277**, 201-226 (1977).
2. Nasar, S.K.T. & Rai, R. Seasonal Fluctuation of the Duration of Meiosis in Rhoeo. *Environ Exp Bot* **25**, 253-256 (1985).
3. Prusicki, M.A. *et al.* Live cell imaging of meiosis in Arabidopsis thaliana. *Elife* **8** (2019).
4. Valuchova, S. *et al.* Imaging plant germline differentiation within Arabidopsis flowers by light sheet microscopy. *Elife* **9** (2020).
5. Kolowerzo-Lubnau, A., Niedojadlo, J., Swidzinski, M., Bednarska-Kozakiewicz, E. & Smolinski, D.J. Transcriptional activity in diplotene larch microsporocytes, with emphasis on the diffuse stage. *PLoS One* **10**, e0117337 (2015).
6. Charalambous, C., Webster, A. & Schuh, M. Aneuploidy in mammalian oocytes and the impact of maternal ageing. *Nat Rev Mol Cell Biol* **24**, 27-44 (2023).

7. Alexander, A.K. *et al.* A-MYB and BRDT-dependent RNA Polymerase II pause release orchestrates transcriptional regulation in mammalian meiosis. *Nat Commun* **14**, 1753 (2023).
8. Bellutti, L. *et al.* Genome-wide transcriptional silencing and mRNA stabilization allow the coordinated expression of the meiotic program in mice. *Nucleic Acids Res* **53** (2025).
9. Gao, J., Qin, Y. & Schimenti, J.C. Gene regulation during meiosis. *Trends Genet* **40**, 326-336 (2024).
10. Jin, L. & Neiman, A.M. Post-transcriptional regulation in budding yeast meiosis. *Curr Genet* **62**, 313-315 (2016).
11. Morgan, M., Kumar, L., Li, Y. & Baptissart, M. Post-transcriptional regulation in spermatogenesis: all RNA pathways lead to healthy sperm. *Cell Mol Life Sci* **78**, 8049-8071 (2021).
12. Brar, G.A. *et al.* High-resolution view of the yeast meiotic program revealed by ribosome profiling. *Science* **335**, 552-557 (2012).
13. Carlile, T.M. & Amon, A. Meiosis I is established through division-specific translational control of a cyclin. *Cell* **133**, 280-291 (2008).
14. Berchowitz, L.E. *et al.* Regulated Formation of an Amyloid-like Translational Repressor Governs Gametogenesis. *Cell* **163**, 406-418 (2015).
15. Jin, L., Zhang, K., Xu, Y., Sternglanz, R. & Neiman, A.M. Sequestration of mRNAs Modulates the Timing of Translation during Meiosis in Budding Yeast. *Mol Cell Biol* **35**, 3448-3458 (2015).
16. da Cruz, I. *et al.* Transcriptome analysis of highly purified mouse spermatogenic cell populations: gene expression signatures switch from meiotic-to postmeiotic-related processes at pachytene stage. *BMC Genomics* **17**, 294 (2016).
17. Susor, A., Jansova, D., Anger, M. & Kubelka, M. Translation in the mammalian oocyte in space and time. *Cell Tissue Res* **363**, 69-84 (2016).
18. Cheng, S. *et al.* Mammalian oocytes store mRNAs in a mitochondria-associated membraneless compartment. *Science* **378**, eabq4835 (2022).
19. Rudzka, M. *et al.* Functional nuclear retention of pre-mRNA involving Cajal bodies during meiotic prophase in European larch (Larix decidua). *Plant Cell* **34**, 2404-2423 (2022).
20. Nelms, B. & Walbot, V. Gametophyte genome activation occurs at pollen mitosis I in maize. *Science* **375**, 424-429 (2022).
21. Cairo, A. *et al.* SMG7 and eIF4A constitute a homeostatic module controlling P-body condensation and function of Meiotic bodies. *bioRxiv*, 2025.2005.2003.652043 (2025).
22. Cairo, A. *et al.* Meiotic exit in Arabidopsis is driven by P-body-mediated inhibition of translation. *Science* **377**, 629-634 (2022).

23. Bulankova, P., Riehs-Kearnan, N., Nowack, M.K., Schnittger, A. & Riha, K. Meiotic progression in Arabidopsis is governed by complex regulatory interactions between SMG7, TDM1, and the meiosis I-specific cyclin TAM. *Plant Cell* **22**, 3791-3803 (2010).
24. Cifuentes, M. *et al.* TDM1 Regulation Determines the Number of Meiotic Divisions. *PLoS Genet* **12**, e1005856 (2016).
25. d'Erfurth, I. *et al.* The cyclin-A CYCA1;2/TAM is required for the meiosis I to meiosis II transition and cooperates with OSD1 for the prophase to first meiotic division transition. *PLoS Genet* **6**, e1000989 (2010).
26. Pomeranz, M.C. *et al.* The Arabidopsis tandem zinc finger protein AtTZF1 traffics between the nucleus and cytoplasmic foci and binds both DNA and RNA. *Plant Physiol* **152**, 151-165 (2010).
27. Lu, P. *et al.* The Arabidopsis CALLOSE DEFECTIVE MICROSPORE1 gene is required for male fertility through regulating callose metabolism during microsporogenesis. *Plant Physiol* **164**, 1893-1904 (2014).
28. Capitao, C. *et al.* A CENH3 mutation promotes meiotic exit and restores fertility in SMG7-deficient Arabidopsis. *PLoS Genet* **17**, e1009779 (2021).
29. Riehs-Kearnan, N., Gloggnitzer, J., Dekrout, B., Jonak, C. & Riha, K. Aberrant growth and lethality of Arabidopsis deficient in nonsense-mediated RNA decay factors is caused by autoimmune-like response. *Nucleic Acids Res* **40**, 5615-5624 (2012).
30. De Storme, N. & Geelen, D. Cytokinesis in plant male meiosis. *Plant Signal Behav* **8**, e23394 (2013).
31. Chai, G. *et al.* Arabidopsis C3H14 and C3H15 have overlapping roles in the regulation of secondary wall thickening and anther development. *J Exp Bot* **66**, 2595-2609 (2015).
32. Kim, W.C. *et al.* AtC3H14, a plant-specific tandem CCCH zinc-finger protein, binds to its target mRNAs in a sequence-specific manner and affects cell elongation in Arabidopsis thaliana. *Plant J* **80**, 772-784 (2014).
33. Klepikova, A.V., Kasianov, A.S., Gerasimov, E.S., Logacheva, M.D. & Penin, A.A. A high resolution map of the Arabidopsis thaliana developmental transcriptome based on RNA-seq profiling. *Plant J* **88**, 1058-1070 (2016).
34. Hardy, E.C. & Balcerowicz, M. Untranslated yet indispensable-UTRs act as key regulators in the environmental control of gene expression. *J Exp Bot* **75**, 4314-4331 (2024).
35. Javorka, P., Raxwal, V.K., Najvarek, J. & Riha, K. artMAP: A user-friendly tool for mapping ethyl methanesulfonate-induced mutations in Arabidopsis. *Plant Direct* **3**, e00146 (2019).
36. Riehs, N. *et al.* Arabidopsis SMG7 protein is required for exit from meiosis. *J Cell Sci* **121**, 2208-2216 (2008).

37. Nakagawa, T. *et al.* Improved Gateway binary vectors: high-performance vectors for creation of fusion constructs in transgenic analysis of plants. *Biosci Biotechnol Biochem* **71**, 2095-2100 (2007).

38. Alexander, M.P. Differential staining of aborted and nonaborted pollen. *Stain Technol* **44**, 117-122 (1969).

39. Yoo, S.D., Cho, Y.H. & Sheen, J. Arabidopsis mesophyll protoplasts: a versatile cell system for transient gene expression analysis. *Nat Protoc* **2**, 1565-1572 (2007).

40. Duncan, S., Olsson, T.S.G., Hartley, M., Dean, C. & Rosa, S. A method for detecting single mRNA molecules in Arabidopsis thaliana. *Plant Methods* **12**, 13 (2016).

41. Duncan, S., Johansson, H.E. & Ding, Y. Reference genes for quantitative Arabidopsis single molecule RNA fluorescence in situ hybridization. *J Exp Bot* **74**, 2405-2415 (2023).

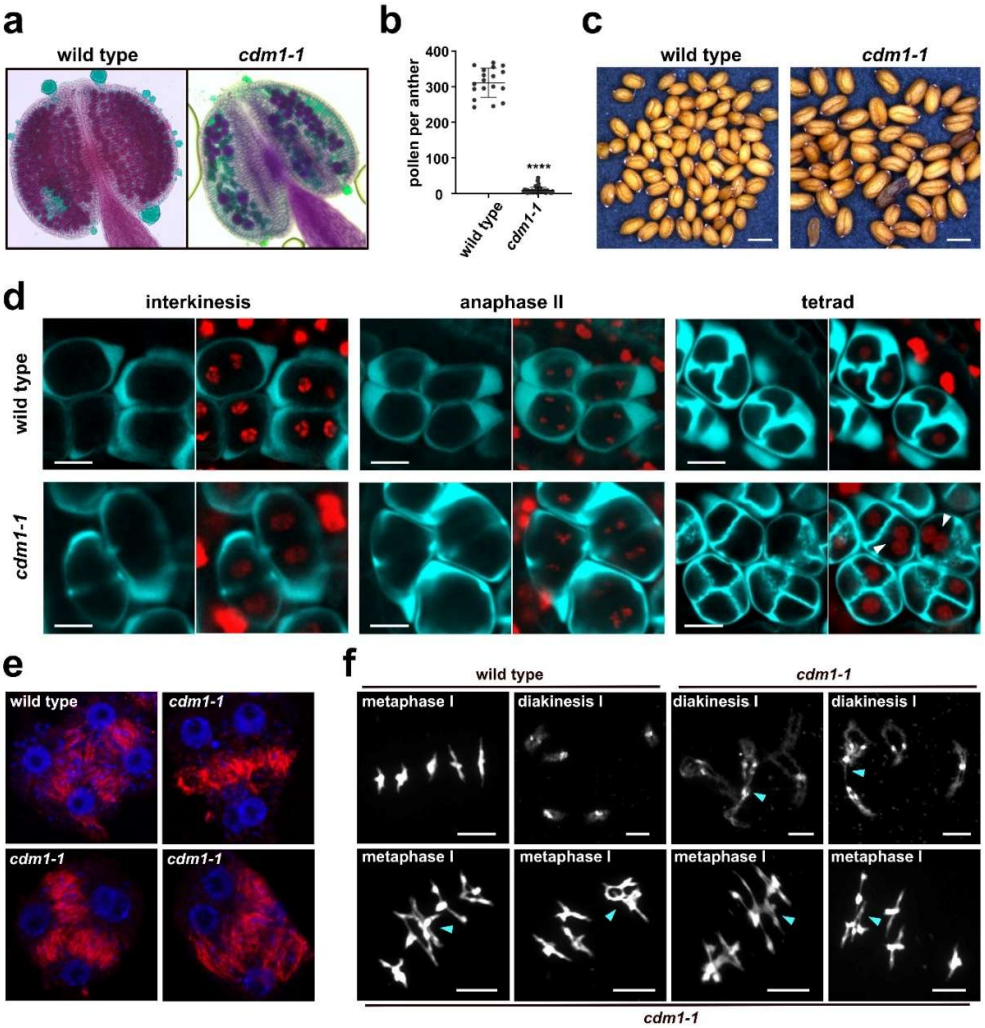

Figure 1. Meiotic and post-meiotic defects in *cdm1-1* mutants. (**a**) Alexander staining of wild type and *cdm1-1* mutant anthers. (**b**) Quantification of pollen viability shown in (a) (unpaired *t*-test, $p < 0.0001$). (**c**) Seeds from wild type and *cdm1-1* mutants (scale = 0.5 mm). (**d**) SR2200 staining of callose (cyan) in meiocytes expresdsing the HTA10-RFP chromatin marker (red), imaged by confocal microscopy (scale = 10 µm). (**e**) Anti-tubulin immunostaining (red) during telophase II showing radial microtubule arrays (RMAs). DNA is counterstained with DAPI (blue). (**f**) Meiotic chromosome spreads stained with DAPI. Association of heterologous bivalents are indicated by blue arrowheads.

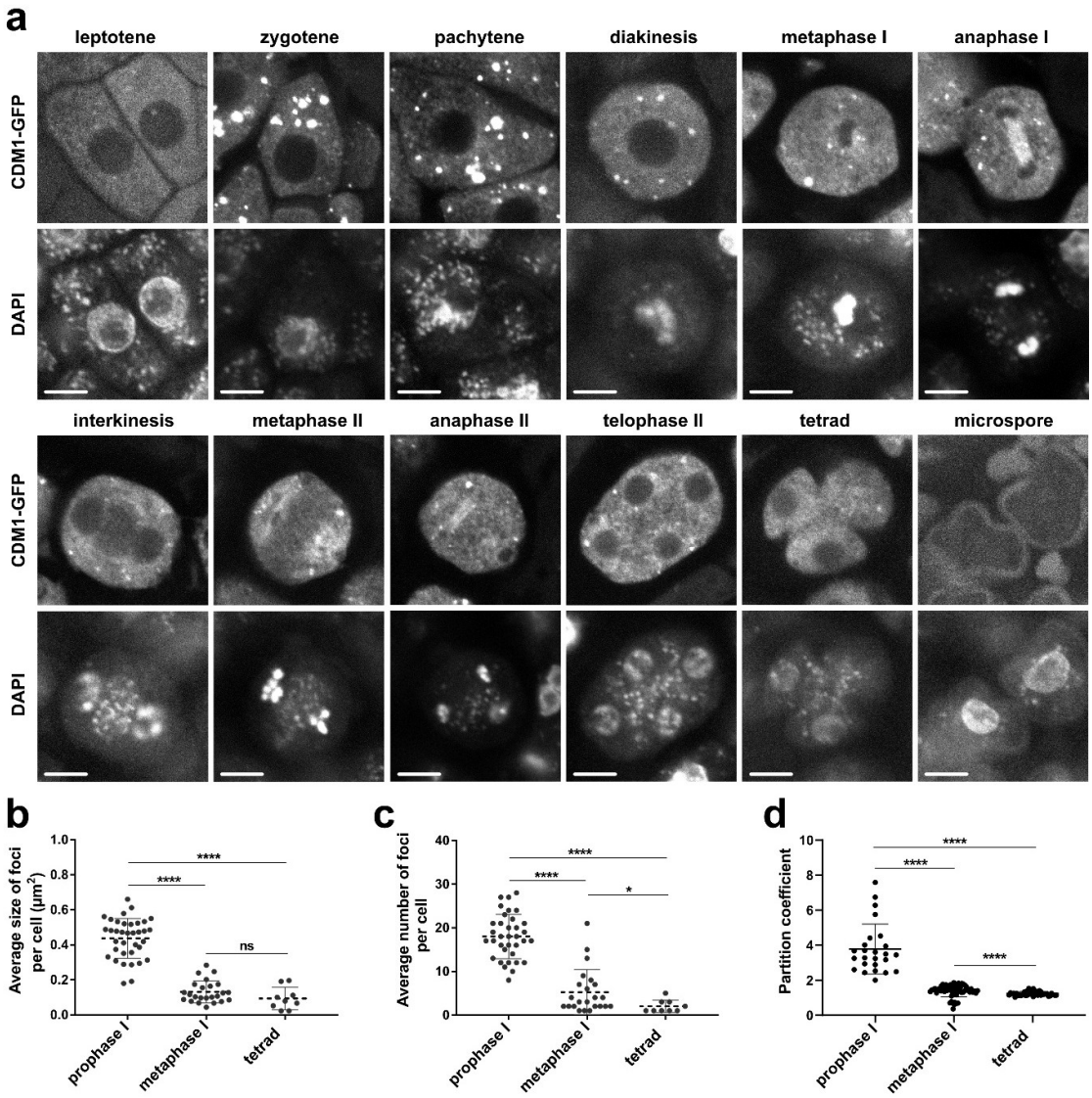

Figure 2. Subcellular localization of CDM1-GFP during male meiosis. (**a**) Confocal micrographs of pollen mother cells expressing CDM1-GFP (scale = 5 µm). (**b-d**) Dot plots showing quantification of the average size of CDM1-GFP foci per cell (b), average number of CDM1-GFP foci per cell (c), and partitioning coefficient of individual foci (d) at indicated meiotic stages. Data were quantified from a single representative confocal layer. Statistical significance of the difference was assessed using unpaired Mann-Whitney test. *P*-values: **** = <0.0001, * = 0.0250, ns = not significant.

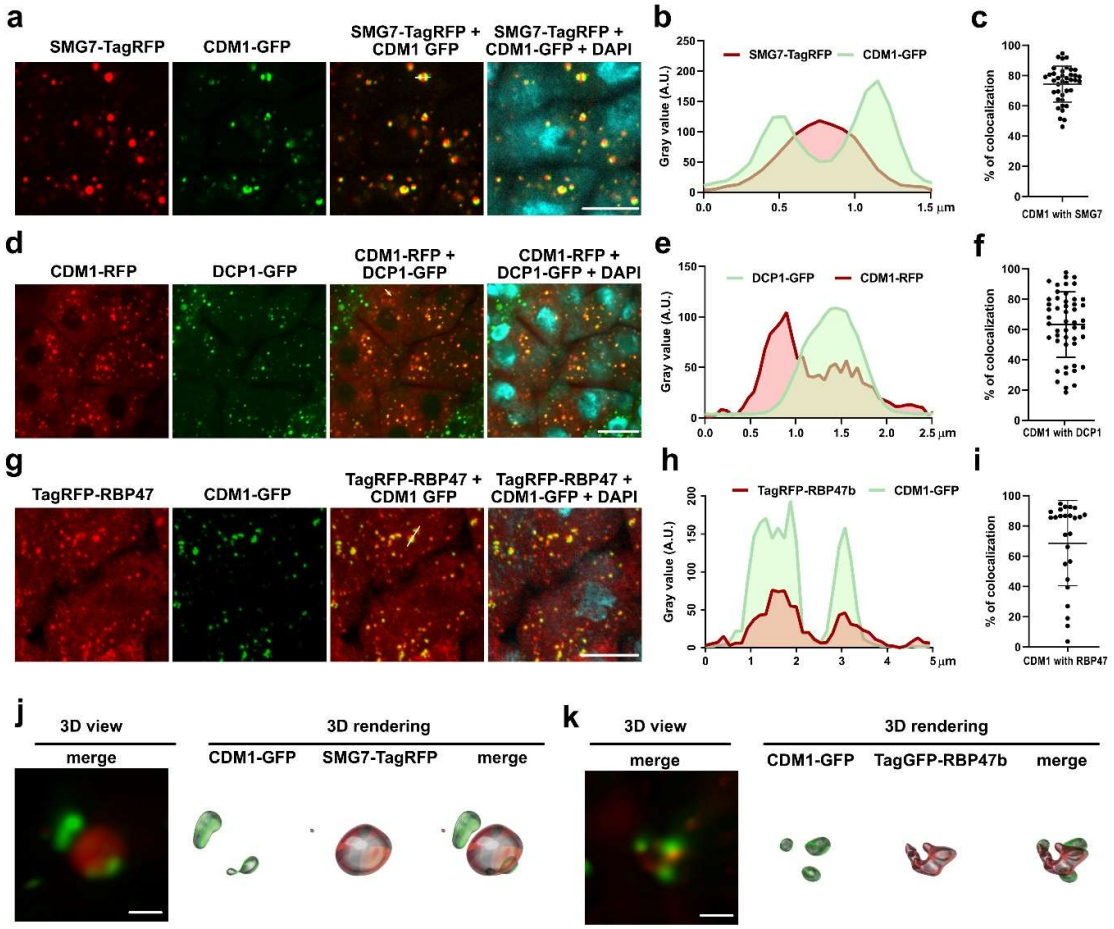

Figure 3. Colocalization of CDM1 with markers of P-bodies and stress granules (**a**) Confocal micrographs of zygotene meiocytes co-expressing CDM1-GFP and SMG7-TagRFP (scale bar = 10 µm). (**b**) Diagram showing superimposed intensity profiles of GFP and TagRFP signals along the line indicating in micrograph (a). (**c**) Dot plot indicating precenting of CDM1 foci co-localizing with SMG7 foci. (**d**) Confocal micrographs of zygotene meiocytes co-expressing CDM1-RFP and GFP (scale bar = 10 µm). (**e**) Diagram showing superimposed intensity profiles of RFP and GFP signals along the line indicating in micrograph (d). (**f**) Dot plot indicating precenting of CDM1 foci co-localizing with DCP1 foci. (**g**) Confocal micrographs of zygotene meiocytes co-expressing CDM1-GFP and TagRFP-RBP47 (scale bar = 10 µm). (**h**) Diagram showing superimposed intensity profiles of GFP and TagRFP signals along the line indicating in micrograph (g). (**i**) Dot plot indicating precenting of CDM1 foci co-localizing with RBP47 foci. (**j,k**) Supper-resolution micrographs of indicated protein condensates visualized by 3D view and 3D rendering using Imaris software (scale bar = 0.5 µm).

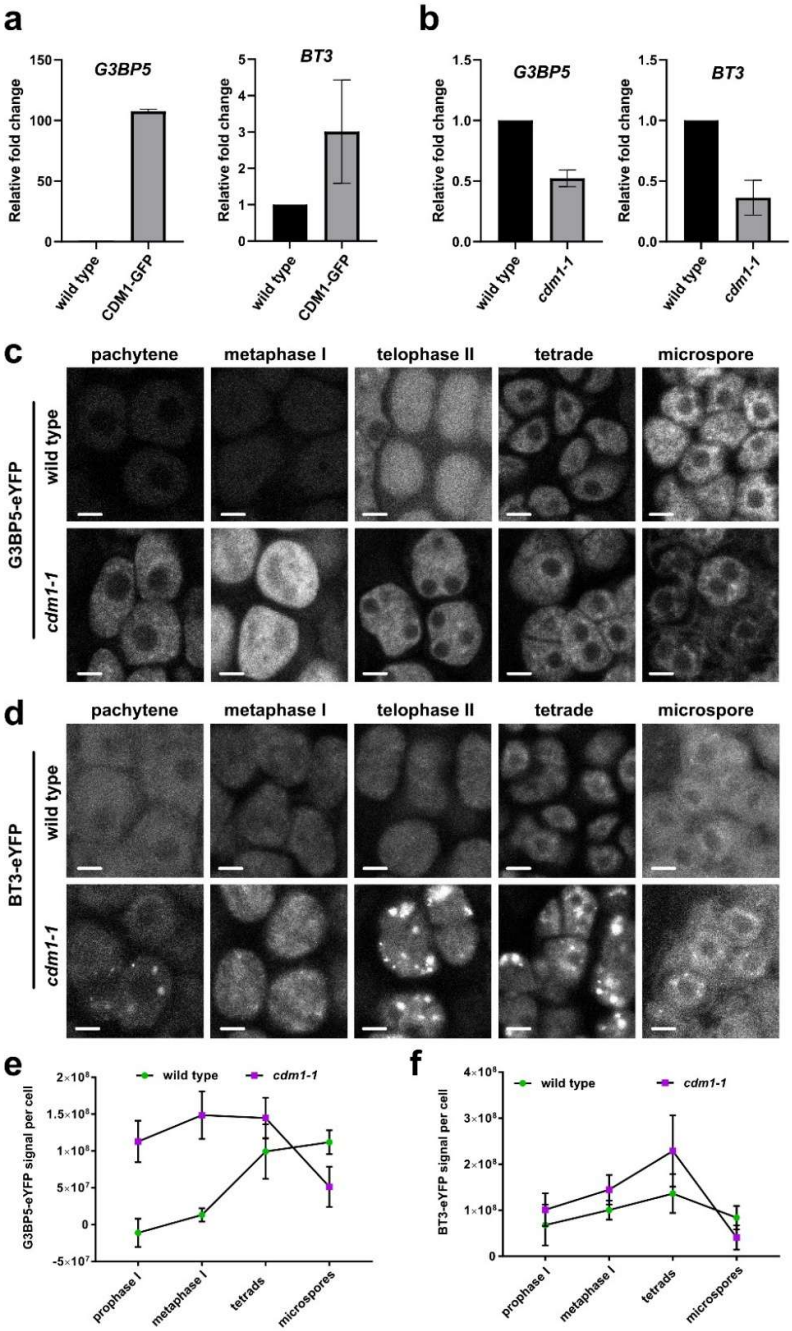

Figure 4. Regulation of *G3BP5* and *BT3* in pollen mother cells by CDM1 (**a**) Bar charts showing enrichment of the indicated mRNAs in anti-GFP immunoprecipitated fractions from wild type and CDM1-GFP plants, as measured by RIP-qPCR. Error bars indicated standard deviations from two biological replicates. (**b**) Relative abundance of *G3BP5* and *BT3* mRNAs in floral buds from wild type and *cdm1-1* plants quantified by RT-qPCR. Error bars indicate SD from three biological replicates. (**c,d**) Confocal micrographs of G3BP5-YFP (c) and BT3-YFP (d) signals in wild type and *cdm1-1* pollen mother cells. All images in (c) and (d) were acquired using identical microscope settings and processed with the same parameters. Images show single representative confocal sections; scale bars = 5 µm. (**e, f**) Quantification of G3BP5-YFP (e) and BT3-YFP (f) total fluorescence intensity per meiocyte.

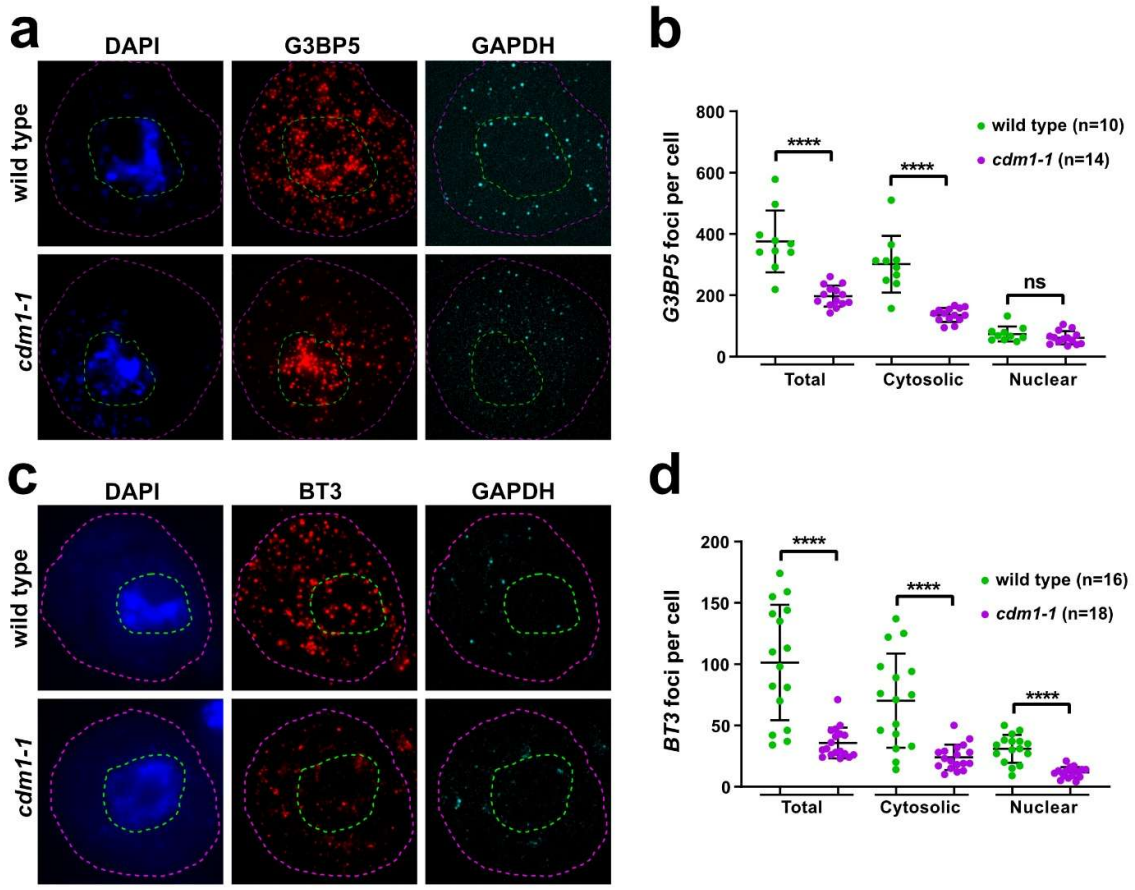

Figure 5. smFISH analysis of *G3BP5* and *BT3* transcripts in wild-type and *cdm1-1* meiocytes. (**a,c**) Micrographs of pachytene meiociytes subject to smFISH with G3BP5 (a) or BT3 (c) probes (red). DNA was counterstained with DAPI (blue), and a probe detecting ubiquitously expressed GAPDH was used as a control (cyan). Magenta dotted lines outline cell boundaries; green dotted lines indicate approximate nuclear boundaries inferred from the DAPI signal. (**b, d**) Quantification of mRNA foci per cell for *G3BP5* (b) and *BT3* (d). Statistical significance was assessed using an unpaired Mann-Whitney test (**** = <0.0001, ns = not significant). Scale bar = 5 µm.

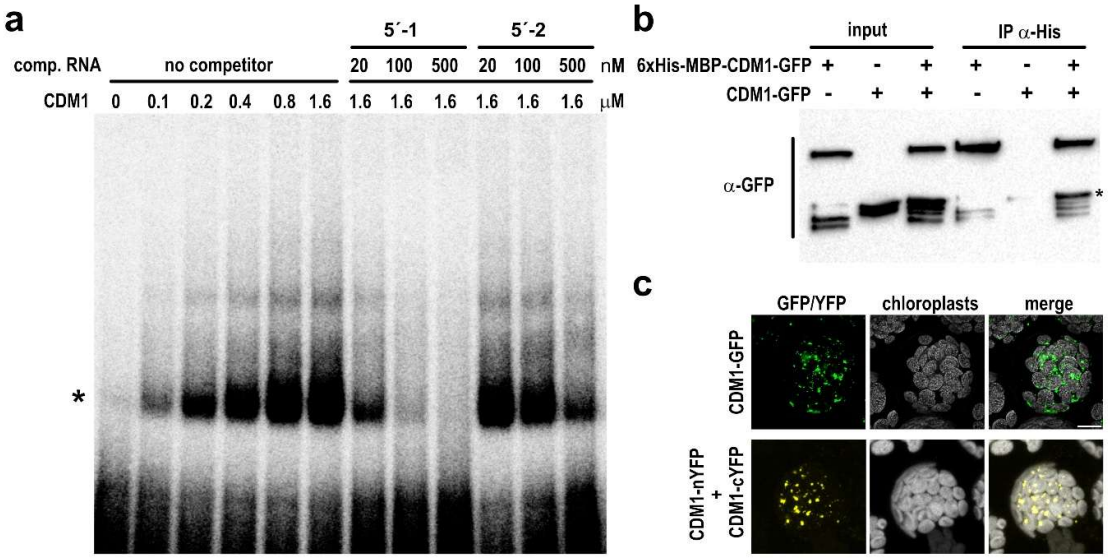

Figure 6: CDM1 directly binds *G3BP5* RNA and self-associates. (**a**) Autoradiogram of REMSA with CDM1 protein and a 20 nM 5´-1 RNA probe spanning the first 75 nucleotides of *G3BP5´* 5´UTR. Unlabeled 5´-1 and 5´-2 RNAs were used as competitors. The asterisk indicates the CDM1-*GRBP5* complex (**b**). Western blot of *in vitro* pull-down assay with 6xHis-MBP-CDM1-GFP and CDM1-GFP proteins using anti-His antibody. Proteins were detected using anti-GFP antibody. The asterisk marks the CDM1-GFP signal. (**c**) Bimolecular fluorescence complementation assay in mesophyll protoplasts. Top panel: micrographs showing CDM1-GFP expression in transfected protoplasts. Bottom panel: YFP fluorescence signal upon co-transfection of CDM1 constructs fused to either N-terminal (CDM1-nYFP) or C-termina (CDM1-cYFP) halves of YFP.

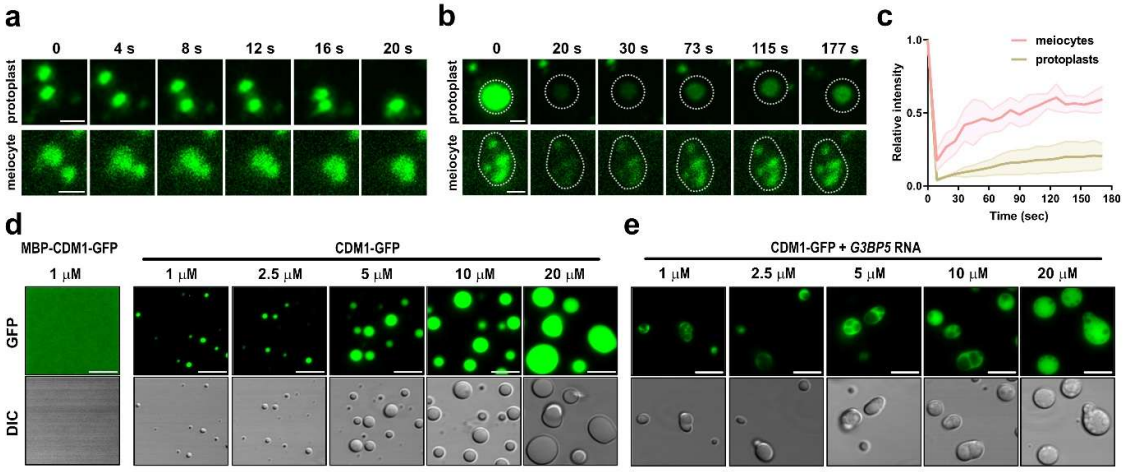

Figure 7. Dynamic properties of CDM1 foci and *in vitro* phase separation of CDM1 protein. (**a**) Time-lapse series showing fusion of two CDM1-GFP foci in protoplasts (top) and meiocytes (bottom). (**b**) FRAP analysis of CDM1-GFP signal in protoplasts (top) and in meiocytes (bottom). Scale bars in (a) and (b) = 1 µm. (**c**) Quantification of CDM1-GFP FRAP in meiocytes and protoplasts. (**d,e**) *In vitro* phase separation assay with increasing concentration of CDM1-GFP, either without (d) or with (e) *G3BP5* RNA (100 ng/µL). Top panels show GFP signal and the bottom panels show the corresponding DIC images. Scale bar = 5 µm.